

Germline genetics, disease, and exposure to medication influence longitudinal dynamics of clonal hematopoiesis

by Taralynn Mack, Yash Pershad, Caitlyn Vlasschaert, Cosmin A. Bejan, Jonathan Brett Heimlich, Yajing Li, Nicole A. Mickels, Joseph C. Van Amburg, Jessica Ulloa, Alexander J. Silver, Leo Y. Luo, Angela Jones, Paul Brent Ferrell, Ashwin Kishtagari, Yaomin Xu, Michael R. Savona, and Alexander G. Bick

Received: August 22, 2024.

Accepted: November 6, 2024.

Citation: Taralynn Mack, Yash Pershad, Caitlyn Vlasschaert, Cosmin A. Bejan, Jonathan Brett Heimlich, Yajing Li, Nicole A. Mickels, Joseph C. Van Amburg, Jessica Ulloa, Alexander J. Silver, Leo Y. Luo, Angela Jones, Paul Brent Ferrell, Ashwin Kishtagari, Yaomin Xu, Michael R. Savona, and Alexander G. Bick. Germline genetics, disease, and exposure to medication influence longitudinal dynamics of clonal hematopoiesis.

Haematologica. 2024 Nov 14. doi: 10.3324/haematol.2024.286513 [Epub ahead of print]

Publisher's Disclaimer.

E-publishing ahead of print is increasingly important for the rapid dissemination of science. Haematologica is, therefore, E-publishing PDF files of an early version of manuscripts that have completed a regular peer review and have been accepted for publication.

E-publishing of this PDF file has been approved by the authors.

After having E-published Ahead of Print, manuscripts will then undergo technical and English editing, typesetting, proof correction and be presented for the authors' final approval; the final version of the manuscript will then appear in a regular issue of the journal.

All legal disclaimers that apply to the journal also pertain to this production process.

Germline genetics, disease, and exposure to medication influence longitudinal dynamics
of clonal hematopoiesis

Taralynn Mack*¹, Yash Pershad*¹, Caitlyn Vlasschaert², Cosmin A. Bejan³, Jonathan
Brett Heimlich⁴, Yajing Li^{5,6}, Nicole A. Mickels¹, Joseph C. Van Amburg¹, Jessica Ulloa¹,
Alexander J. Silver^{4,7}, Leo Y. Luo⁸, Angela Jones¹, Paul Brent Ferrell⁹, Ashwin Kishtagari^{4,10},
Yaomin Xu^{5,6}, Michael R. Savona^{4,7,10,11}, Alexander G. Bick^{1,12}

*T.M. and Y.P. contributed equally

¹ Vanderbilt Genetics Institute, Vanderbilt University, Nashville, TN, USA,

²Department of Medicine, Queen's University, Kingston, Ontario, Canada, ³Department of

Biomedical Informatics, Vanderbilt University Medical Center, Nashville, TN, USA, ⁴

Department of Medicine, Vanderbilt University Medical Center, Nashville, TN, USA, ⁵

Department of Biomedical Informatics, Vanderbilt University Medical Center, Nashville, TN,

USA, ⁶ Department of Biostatistics, Vanderbilt University Medical Center, Nashville, TN, USA,

⁷Program in Cancer Biology, Vanderbilt University School of Medicine, Nashville, TN, USA, ⁸

Department of Radiation Oncology, Vanderbilt University Medical Center, Nashville, TN, USA,

⁹Division of Hematology and Oncology, Department of Medicine, Vanderbilt University

Medical Center, Nashville, TN, USA, ¹⁰ Vanderbilt Ingram Cancer Center, Vanderbilt University

Medical Center, Nashville, TN, USA, ¹¹ Center for Immunobiology, Vanderbilt University

Medical Center, Nashville, TN, USA, ¹² Division of Genetic Medicine, Vanderbilt University

Medical Center, Nashville, Tennessee, USA

Correspondence to: Dr. Alexander Bick, Vanderbilt University Medical Center, 550 Robinson

Research Building, 2200 Pierce Ave, Nashville, TN 37232, alexander.bick@vumc.org

Declarations of Interests

A.G.B. has received honoraria for advisory board membership from, and holds equity in, TenSixteen Bio. M.R.S. has received honoraria for advisory board membership or consultancy from Bristol Myers Squibb, CTI, Forma, Geron, GlaxoSmithKline/Sierra Oncology, Karyopharm, Ryvu Therapeutics, and Taiho Pharmaceutical; has received research funding from ALX Oncology, Astex Pharmaceuticals, Incyte Corporation, Takeda, and TG Therapeutics; holds equity in Empath Biosciences, Karyopharm, and Ryvu Therapeutics; and has been reimbursed for travel expenses by Astex. A.K. has received honoraria for advisory board membership or consultancy from Geron, Sobi, Incyte Corporation, Morposys, Rigel, and Servier Pharmaceuticals.

Author Contributions

These authors contributed equally: Taralynn Mack and Yash Pershad. T.M. and A.G.B. conceived of the study. T.M., Y.P., and C.V. processed the targeted sequencing results to call CHIP mutations and germline genetics. T.M. and Y.P. performed the human genetic association and phenotypic analyses. Y.P., C.A.B., and N.M. performed medications analyses. Y.L., A.K., and Y.X. performed mCA detection. A.J., J.V.A., and J.U. performed sequencing of the samples. J.B.H., A.J.S., L.Y.L., P.B.F., A.K., and M.R.S. provided important feedback to improve the analysis. T.M., Y.P., and A.G.B. wrote the manuscript with input from all authors. A.G.B. supervised the work. All authors read, revised and approved the manuscript.

Data Availability

Supplemental table of CHIP mutations and variant allele fractions is available on GitHub: https://github.com/bicklab/mtp/blob/main/Mack_Pershad_s01.txt. Raw sequencing data will be made available on dbGaP upon publication.

Funding

This work was supported by NIH grant DP5 OD029586, a Burroughs Wellcome Fund Career Award for Medical Scientists, an E.P. Evans Foundation grant, a RUNX1 Research Program grant, a Pew Charitable Trusts and Alexander and Margaret Stewart Trust Pew-Stewart Scholar for Cancer Research award, a Vanderbilt University Medical Center Brock Family Endowment grant, and a Young Ambassador Award (A.G.B.); NIH grant T32 GM007347 (Y.P., A.J.S.); National Institutes of Health grant F30 DK127699 (A.J.S.); NIH grant K12 CA090625 (L.Y.L.), the Adventure Alle Fund fund, a Beverly and George Rawlings Endowment, and NIH grants R01 CA262287 and U01 OH012271 (M.R.S.). Research at the Vanderbilt-Ingram Cancer Center is supported by NIH grant P30 CA068485. Vanderbilt University Medical Center's BioVU projects are supported by numerous sources: institutional funding, private agencies, and federal grants. These include NIH funded Shared Instrumentation Grant S10OD017985, S10RR025141, and S10OD025092; CTSA grants UL1TR002243, UL1TR000445, and UL1RR024975.

Code Availability

Code for the analyses of this paper can be found here: <https://github.com/bicklab/mtp>. The code to call mosaic chromosomal alterations with MoChA is available here:

<https://github.com/freeseek/mocha>. Code for Mutect2-GATK can be found here:

<https://gatk.broadinstitute.org/hc/en-us/articles/360037593851-Mutect2>. Code to call germline

SNPs using the targeted assay can be found here: [https://github.com/gatk-workflows/gatk4-](https://github.com/gatk-workflows/gatk4-germline-snps-indels)

[germline-snps-indels](https://github.com/gatk-workflows/gatk4-germline-snps-indels). Code to perform PheWAS analysis can be found here:

<https://github.com/MASILab/pyPheWAS>.

Main

Clonal hematopoiesis of indeterminate potential (CHIP) occurs when a hematopoietic stem cell acquires a somatic driver mutation in a leukemia-associated gene, with a variant allele fraction (VAF) exceeding 2% in peripheral blood.¹ Higher VAF is associated with increased morbidity and mortality risk.²⁻⁵ Identifying factors influencing clonal expansion rate is crucial for risk stratification in CHIP patients. Recent cost-effective targeted assays have enabled serial sequencing and longitudinal profiling of CHIP dynamics.⁶ We present the largest longitudinal analysis of CHIP mutational dynamics to-date, examining 3,000 individuals from the Vanderbilt BioVU biobank. Our findings reveal that CHIP growth rates vary significantly by driver gene and are influenced by germline variants and medication exposures. Additionally, we demonstrate that monitoring blood counts may be more informative for risk stratification than frequent resequencing in CHIP patients.

We performed targeted, error-corrected sequencing on serial blood samples from 3,000 individuals in the Vanderbilt BioVU biobank, using custom-designed probes for 22 CHIP-associated genes (**Supplementary Table 1; Supplementary Figure 1**). Vanderbilt University Medical Center's Institutional Review Board oversees BioVU and approved this project (IRB #201783). Unique molecular identifiers (UMI) were used for error correction, excluding mutations detected from a single UMI. The mean coverage depth was 1725x after de-duplication. CHIP mutations were called for variants with $\geq 100x$ total read depth, ≥ 3 variant allele reads, and $>2\%$ VAF in at least one blood draw. We identified 893 CHIP mutations in 711 individuals (**Figure 1A**). The mean age of the participants at the first blood draw was 70 (range: 19-96). Participants' mean age at first draw was 70 years (range: 19-96), with a mean 5.7-year interval (range: 0.7-13) between samples. Mean VAFs were 6.7% and 9.5% at first and second draws,

respectively. Most individuals (79%) had a single CHIP mutation, 16% had two, and 4% had three or more (**Figure 1B**). *DNMT3A* and *TET2* were the most frequently mutated genes. Of the 711 individuals, 74% had CHIP at both timepoints, while 26% had >2% VAF at only one draw, predominantly (78%) at the second draw.

We modeled the growth rate r with a compound interest formula $r = \frac{VAF_2^{1/time}}{VAF_1} - 1$.

SRSF2/SF3B1 (splicing factor) driver mutations exhibited the fastest average growth rate (~25% annually), while *DNMT3A* driver mutations showed the slowest rate (~7% annually) (**Figure 1C**). 78% of mutations increased in VAF (annual growth rate > 1%), consistent with prior studies.^{5,7} Decreases in VAF (annual growth rate < -1%) were observed in 30% of *JAK2*, 21% of *ASXL1*, 25% of *DNMT3A*, 19% of *PPM1D*, 19% of *TET2*, and 0% of *SRSF2/SF3B1* mutations. While certain driver genes are more prone to expansion, CHIP expansion rates varied considerably among individuals with the same driver gene. This variability may necessitate larger sample sizes in prospective randomized controlled trials aiming to identify drugs that slow expansion.

We analyzed individuals with two CHIP mutations, which may co-occur as subclones or in distinct cells (**Figure 1D**). Mutation pairs were classified as subclones if their growth rates were within 0.6 standard deviations of each other; otherwise, they were considered distinct. Of 116 individuals with two mutations, 66 (57%) had subclones. Subclones showed significantly lower growth rates than distinct clones ($\beta = -0.15$, $P = 0.02$) (**Figure 1E**). This finding was robust for multiple definitions of distinct versus subclones (standard deviation thresholds ranging from 0.4 to 0.8). Co-occurrence analysis of CHIP mutations by driver gene (**Figure 1F**) revealed that *JAK2* and *SF3B1/SRSF2* co-occurred significantly more often than expected (OR=48.7,

p=0.0006). Two mutations in *TET2* (OR=6.6, p=0.001), *DNMT3A* (OR=3.8, p=0.006), and *PPM1D* (OR=8.7, p=0.02) also occurred more frequently than chance. Conversely, *DNMT3A* and *TET2* co-occurred less often than expected based on frequency (OR=0.4, p=0.02) (**Figure 1G**).

We investigated individual determinants of CHIP expansion rate. When accounting for driver gene mutations, growth rate showed no significant association with age (P = 0.07), body mass index (P = 0.68), biological sex (P = 0.89), or smoking status (P = 0.70). Our targeting assay included probes for germline variants previously linked to CHIP prevalence and estimated growth rate (**Figure 2A**).^{1,8} Each additional G allele in rs1800057 (ATM) correlated with increased growth rate ($\beta = 0.46$, 95% CI: 0.23 to 0.67, P<0.001, **Figure 2B**), potentially explaining its association with CHIP prevalence.¹ Consistent with NHLBI's TOPMed cohort findings,⁹ each T allele at rs2887399 (in the *TCL1A* promoter) associated with increased *DNMT3A* expansion rate (P=0.04) and decreased *TET2* expansion rate (P=0.02) (**Figure 2C**).

We investigated associations between medication exposure duration and CHIP growth rate. While no medications showed significant associations after multiple hypothesis correction, several demonstrated suggestive effects (**Figure 2D**). Three drugs suggested reduced annual growth rates: colchicine ($\beta = -3.5\%$, 95% CI: -0.5% to -7%, P=0.03), denosumab ($\beta = -2.5\%$, 95% CI: -0.3% to -5%, P=0.03), and methylprednisolone ($\beta = -1.0\%$, 95% CI: -0.4% to -2%, P=0.01). These associations have biological plausibility: methylprednisolone has anti-inflammatory effects, colchicine may abrogate cardiovascular risk in *TET2* CHIP, and denosumab inhibits RANKL, which *DNMT3A*-mutated monocytes overexpress in bone.¹⁰ Conversely, hydroxychloroquine suggested increased annual growth rate ($\beta = 3.1\%$, 95% CI: -0.3% to 5%, P=0.03). Moreover, we performed 3:1 case-control matching by age, sex, CHIP

driver gene, baseline VAF, and drug indication for each drug and tested the association with growth rate. In this sensitivity analysis, we observe an association between exposure duration between sequencing timepoints of colchicine and methylprednisolone and decreased growth rate. In external validation cohort Clonal Hematopoiesis and Inflammation in the Vasculature (CHIVE)¹¹, 4/5 mutations exposed to colchicine and 8/10 exposed to methylprednisolone showed reduced or unchanged VAF (**Supplementary Figures 2**). We found no associations between pre-existing diagnoses and CHIP expansion rate (**Figure 2E**). The lack of association between preexisting atherosclerosis and CHIP growth rate supports a unidirectional association between clonal hematopoiesis and atherosclerosis.¹²

We investigated the consequences of CHIP expansion rate on blood counts and diagnoses after the second blood draw. Analyzing associations between growth rate and time to blood cell count abnormalities (as per Niroula et al.¹³), we found that rank-inverse normalized growth rate, adjusted for age, initial VAF, and sex, was associated with shorter time to high myeloid cell parameters (HR = 1.14, 95% CI 1.02-1.27) and low myeloid cell parameters (HR = 1.20, 95% CI 1.05-1.36). No associations were found with lymphocytosis (P=0.48) or lymphopenia (P=0.53). Annual growth rate >16% increased risk of both high and low myeloid cell parameters (P=0.003 and P<0.001, respectively) (**Figure 3A**). A 1% increase in annual growth rate suggested a 1.6-fold increased risk of myeloproliferative disorders (95% CI: 1.1-2.5, P=0.02), though this was not significant after multiple-hypothesis correction (**Figure 3B**). These findings indicate that growth rate signals heightened disease risk in individuals with CHIP.

We next examined changes in clinical risk scores over time, focusing on the Clonal Hematopoiesis Risk Score (CHRS) for 138 individuals with complete blood count data within 6 months of sequencing.¹⁴ Of 115 individuals initially classified as low risk (CHRS \leq 9.5), 24

(21%) were reclassified as intermediate risk ($10 < \text{CHRS} < 12$) at the second blood draw (**Figure 3C**). Among 21 initially intermediate-risk individuals, 4 (19%) were reclassified as low risk, and 1 (5%) as high risk ($\text{CHRS} \geq 12.5$). Only 2 individuals were classified as high risk overall. Risk category changes were primarily driven by alterations in blood counts (**Figure 3D**). All individuals with CHRS category changes showed alterations in RDW, MCV, or blood counts, while only 5 (17%) exceeded the 20% VAF threshold, all of whom also had blood count changes. These findings suggest that repeated blood sequencing may be unnecessary without accompanying laboratory abnormalities.

Our study has notable limitations. Despite being the largest cohort of longitudinal CHIP clonal dynamics to-date, we lack power to detect clinical consequences of CHIP growth rate due to the short inter-draw interval and low-risk population. The exclusion of individuals with hematologic malignancies further limits our ability to detect associations between CHIP growth rate and these phenotypes. Additionally, associations between medication exposure and growth rate are susceptible to confounding by indication, although we observed no associations between pre-existing diagnoses and growth rate for the medications of interest and colchicine and methylprednisolone had a significant negative association in matched controls.

In conclusion, we present the largest longitudinal study of CHIP dynamics to date. Our findings demonstrate that germline genetics, medications, driver genes, and mutation numbers significantly influence CHIP growth rates, with considerable individual variation. As targeted CHIP panels become more accessible, clinicians may leverage these identified risk factors and CHIP trajectories to better assess clinical risk in individuals with CHIP.

References

1. Bick AG, Weinstock JS, Nandakumar SK, et al. Inherited causes of clonal haematopoiesis in 97,691 whole genomes. *Nature*. 2020;586(7831):763-768.
2. Jaiswal S, Natarajan P, Silver AJ, et al. Clonal Hematopoiesis and Risk of Atherosclerotic Cardiovascular Disease. *N Engl J Med*. 2017;377(2):111-121.
3. Jaiswal S, Fontanillas P, Flannick J, et al. Age-Related Clonal Hematopoiesis Associated with Adverse Outcomes. *N Engl J Med*. 2014;371(26):2488-2498.
4. Vlasschaert C, Mack T, Heimlich JB, et al. A practical approach to curate clonal hematopoiesis of indeterminate potential in human genetic data sets. *Blood*. 2023;141(18):2214-2223.
5. Fabre MA, de Almeida JG, Fiorillo E, et al. The longitudinal dynamics and natural history of clonal haematopoiesis. *Nature*. 2022;606(7913):335-342.
6. Mack T, Vlasschaert C, Von Beck K, et al. Cost-effective and scalable clonal hematopoiesis assay provides insight into clonal dynamics. *J Mol Diagn*. 2024;26(7):563-573.
7. Uddin MM, Zhou Y, Bick AG, et al. Longitudinal profiling of clonal hematopoiesis provides insight into clonal dynamics. *Immun Ageing*. 2022;19(1):23.
8. Kessler MD, Damask A, O'Keeffe S, et al. Common and rare variant associations with clonal haematopoiesis phenotypes. *Nature*. 2022;612(7939):301-309.
9. Weinstock JS, Gopakumar J, Burugula BB, et al. Aberrant activation of TCL1A promotes stem cell expansion in clonal haematopoiesis. *Nature*. 2023;616(7958):755-763.
10. Wang H, Divaris K, Bohu P, et al. Clonal hematopoiesis driven by mutated DNMT3A promotes inflammatory bone loss. *Cell*. 2024;187(14):3690-3711.e19.
11. Shannon ML, Heimlich JB, Olson S, et al. Clonal Hematopoiesis and Inflammation in the

VasculaturE (CHIVE): a prospective, longitudinal cohort and biorepository. *Blood Adv.* 2024;8(13):3453-3463.

12. Díez-Díez M, Ramos-Neble BL, De La Barrera J, et al. Unidirectional association of clonal hematopoiesis with atherosclerosis development. *Nat Med.* 2024;30(10):2857-2866.
13. Niroula A, Sekar A, Murakami MA, et al. Distinction of lymphoid and myeloid clonal hematopoiesis. *Nat Med.* 2021;27(11):1921-1927.
14. Weeks LD, Niroula A, Neuberg D, et al. Prediction of Risk for Myeloid Malignancy in Clonal Hematopoiesis. *NEJM Evid.* 2023;2(5):10.

Figure Captions

Figure 1: Cohort characteristics and co-occurring clonal hematopoiesis of indeterminate potential (CHIP) mutations.

(A) Our cohort consists of 892 CHIP mutations in 711 individuals. We calculated growth rate using a compound interest formula for sequencing at two blood draws.

(B) Larger bar plot demonstrates the number of CHIP with a mutation in a driver gene. Smaller bar plot shows the number of individuals with 1, 2, 3, and 4 CHIP mutations.

(C) Box plot of growth rate, calculated with a compound interest formula, for each CHIP mutation by driver gene with number of individuals with mutations in the driver gene shown below the gene name. Red diamond represents the mean growth rate. Box represents the interquartile range of the growth rate. Middle line in the box represents the median of the growth rate.

(D) Theoretical example of possible trajectories for individuals with two CHIP mutations. The mutations can either be in distinct cell populations or the same cell population. Variant allele fraction (VAF) trajectories for each of these scenarios should follow similar trends to this example. Each mutation is represented by color, and the line represents change in VAF between first and second blood draws.

(E) Box plot showing the difference in average growth rate of the fastest growing mutations for the 116 individuals grouped into the distinct vs sub-clone categories. The red diamond represents the average of the growth rate. Box represents the interquartile range of the growth rate. Middle line in the box represents the median of the growth rate. The x-axis is the growth rate while the y-axis is the category.

(F) Upset plot showing the different combinations of driver genes represented within the group of 116 individuals with multiple CHIP mutations. Above the upset plot is a bar plot showing the distribution between distinct vs sub-clone trajectories for each of the driver gene combinations, with driver gene on the x-axis and count on the y-axis.

(G) Heat map showing the deviation from random for the co-occurrence of each driver gene pair for the 116 individuals with 2 CHIP mutations. Each gene pair was tested with a Fisher's exact test to identify deviation from expected occurrence via random chance. The x and y-axes represent each gene in a pair, the color of the box represents the direction of the deviation from random, and the darkness of the hue represents the magnitude of the deviation. For gene combinations with a p-value >0.05 , the odds ratio is displayed, and the box is marked with “*” and for gene combinations that passed multiple-hypothesis correction with a p-value of <0.001 , the odds ratio is displayed and the box is marked with “***”.

Figure 2: Determinants of clonal hematopoiesis of indeterminate potential (CHIP) growth rate.

(A) Forest plot of change in annual growth rate (%/year) with each additional copy of the alternate allele (alt allele) for select germline single nucleotide polymorphisms (SNPs) detectable with the targeted sequencing assay among individuals with CHIP mutations. Effect estimate represents the coefficient of a linear regression of growth rate and number of alternate alleles modeled additively as 0, 1, or 2, adjusting for age, sex, race, and variant allele fraction at first sequencing. We computed the 95% confidence interval (95% CI) as the Effect Estimate \pm 1.96

* Standard Error. The p-value tests the null hypothesis of the effect estimate being 0.

(B) Violin plot of annual growth (%/year) for 0 versus > 1 G allele for germline variant chr11:108272729:C:G in *ATM*. When modeled additively, each additional G allele is associated with greater annual growth rate (%/year) in multiple linear regression by 0.46% per year (95% CI: 0.23 to 0.67, $P < 0.001$). There were 619 CHIP mutations in individuals with 0 G alleles, 26 in individuals with 1 G allele, and 2 in individuals with 2 G alleles.

(C) Violin plot of annual growth (%/year) for 0, 1, and 2 T alleles for germline variant chr14:95714358:G:T in *TCL1A* for *DNMT3A* CHIP (left) and *TET2* CHIP (right). When modeled additively, each additional T allele is associated with greater annual growth rate (%/year) for *TET2* CHIP mutations ($P = 0.03$), but not for *DNMT3A* CHIP mutations ($P = 0.49$). There were 132 *TET2* mutations in individuals with 0 T alleles, 54 *TET2* mutations in individuals with 1 T allele, and 6 *TET2* mutations with 2 T alleles. There were 158 *DNMT3A* mutations in individuals with 0 T alleles, 95 *DNMT3A* mutations in individuals with 1 T allele, and 28 *DNMT3A* mutations in individuals with 2 T alleles.

(D) Forest plot of change in annual growth rate (%/year) with each additional prescription month of 4 select drugs with suggestive associations: colchicine, denosumab, methylprednisolone, and hydroxychloroquine. Black effect estimate represents the coefficient of a linear regression of growth rate and number of months exposed to the drug adjusting for age, sex, race, and variant allele fraction at first sequencing with all data. Gray effect estimate represents the coefficient of a linear regression of growth rate and number of months exposed to the drug for 3:1 matched non-drug-exposed controls to drug-exposed cases (matched by age, sex, CHIP driver gene, variant allele fraction at first sequencing). We computed the 95% confidence interval (95% CI) as the Effect Estimate $\pm 1.96 * \text{Standard Error}$. The p-value tests the null hypothesis of the effect estimate being 0. N represents the number of individuals prescribed the drug for at least 1 month.

(E) Forest plot of change in annual growth rate (%/year) among individuals with select pre-existing diagnoses based on phecodes. Individuals had to have their first diagnosis of the phecode before their second blood draw. Estimate represents the coefficient of a linear regression of growth rate and presence of diagnosis as a binary variable adjusting for age, sex, race, and variant allele fraction at first sequencing. We computed the 95% confidence interval (95% CI) as the Effect Estimate $\pm 1.96 * \text{Standard Error}$. The p-value tests the null hypothesis of the effect estimate being 0. N represents the number of individuals with the diagnosis in each regression.

Figure 3: Phenotypic consequences of growth rate

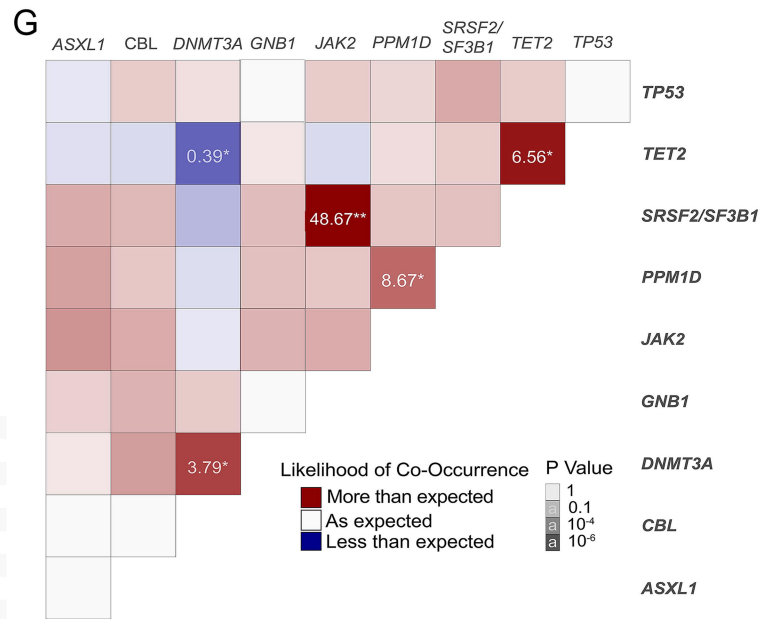
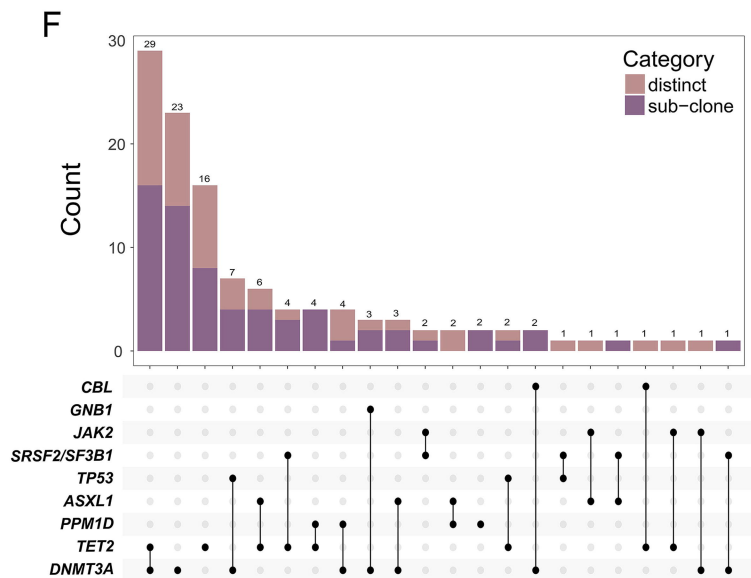
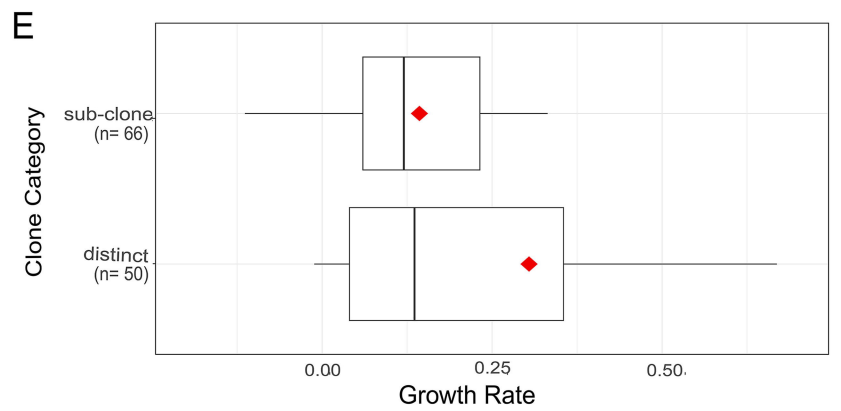
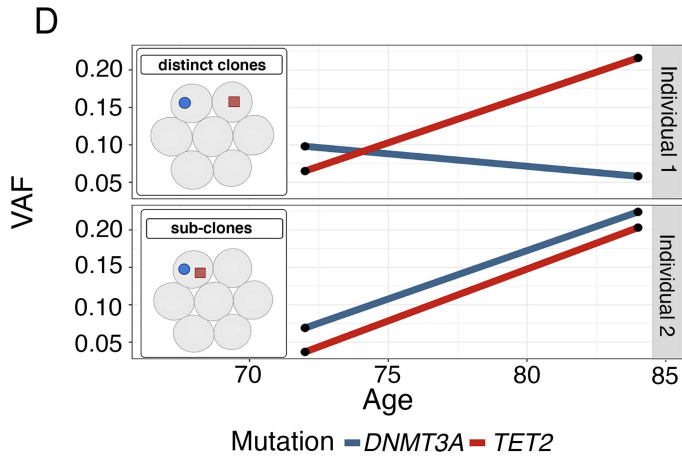
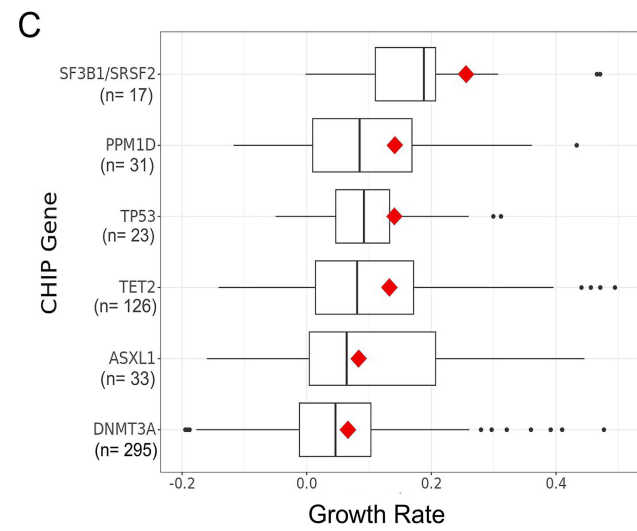
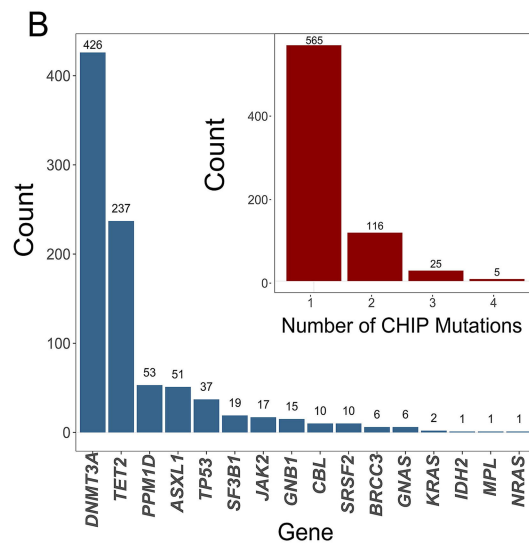
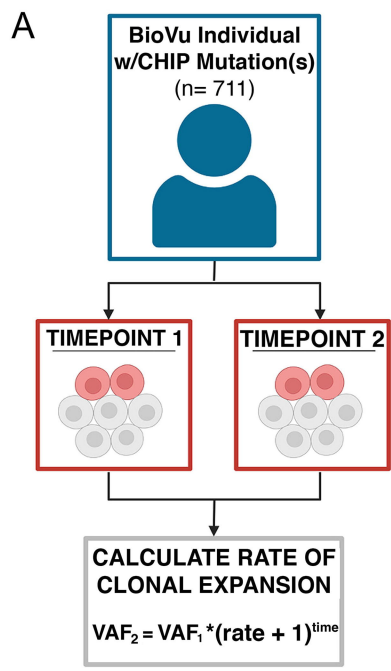
(A) On the left, Kaplan-Meier curve of time to low myeloid counts – defined as thrombocytopenia (platelet count $< 169.06 \times 10^9$ cells/L), anemia (red blood cell count $< 3.96 \times 10^{12}$ cells/L) or neutropenia (neutrophil count $< 1.47 \times 10^9$ cells/L) for individuals with a CHIP growth rate $> 16\%$ annually (red) and $< 16\%$ annually (gray). A Cox proportional hazard model of time to low myeloid counts and rank-inverse normalized growth rate, when adjusting for age, variant allele fraction (VAF) at the first blood draw, and sex was significant (HR = 1.20, 95% CI 1.05-1.36, $P < 0.001$). On the right, Kaplan-Meier curve of time to high myeloid counts – defined as thrombocytosis (platelet count $> 397.1 \times 10^9$ cells/L), polycythemia (red blood cell counts $> 5.5 \times 10^{12}$ cells/L), or elevated neutrophil count (neutrophil count $> 7.06 \times 10^9$ cells/L) for individuals with a CHIP growth rate $> 16\%$ annually (red) and $< 16\%$ annually (gray). A Cox proportional hazard model of time to high myeloid counts and rank-inverse normalized growth rate, when adjusting for age, VAF at the first blood draw, and sex was significant (HR = 1.14, 95% CI 1.02-1.27, $P = 0.003$).

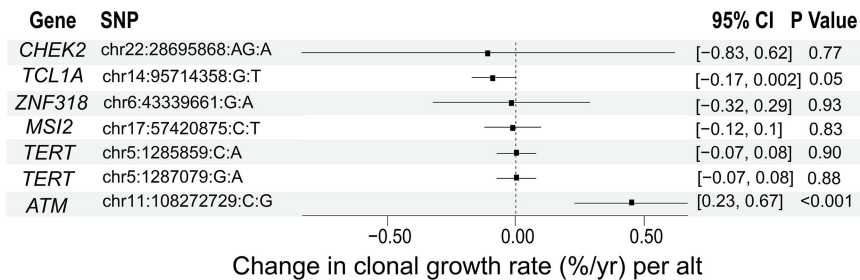
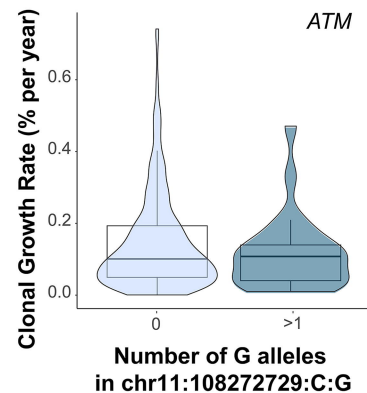
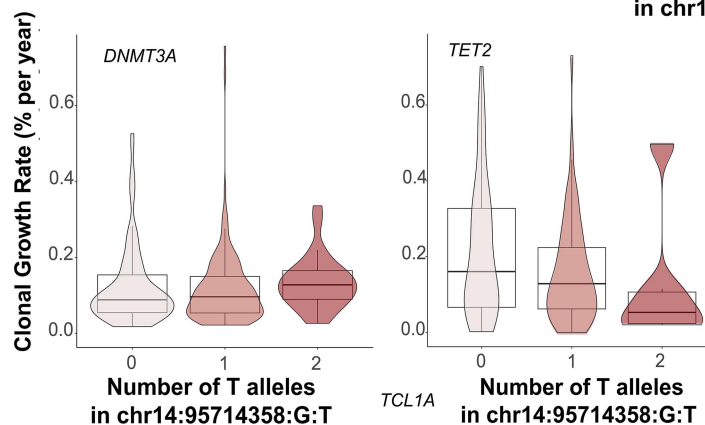
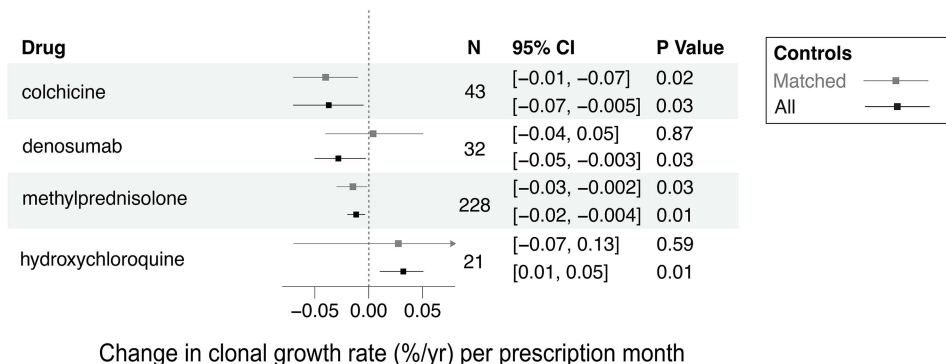
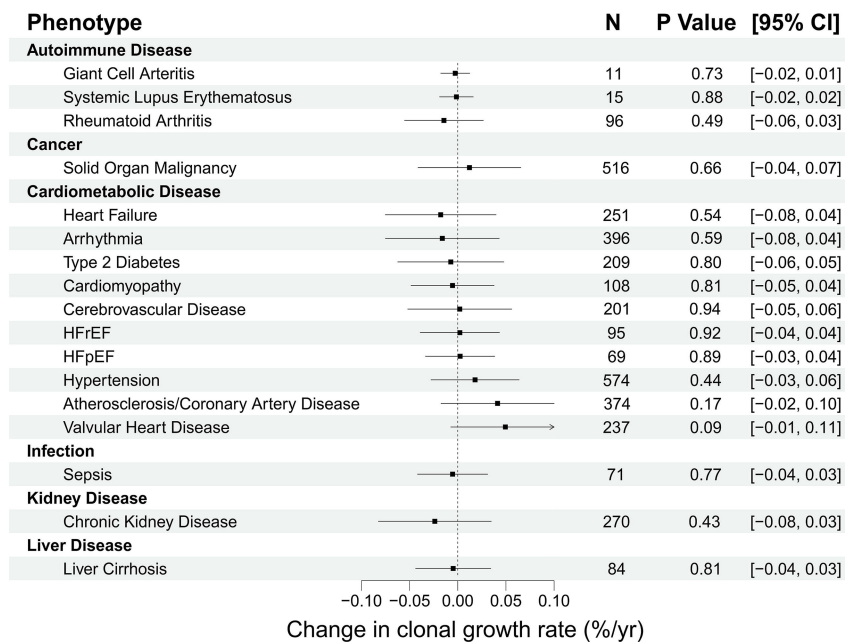
(B) Forest plot showing the association between growth rate and time to event for the listed phenotypes. Out of the 711 individuals in the study, individuals who had a phenotype for the first

time after the second blood draw are included, with each phenotype sample size listed in the figure.

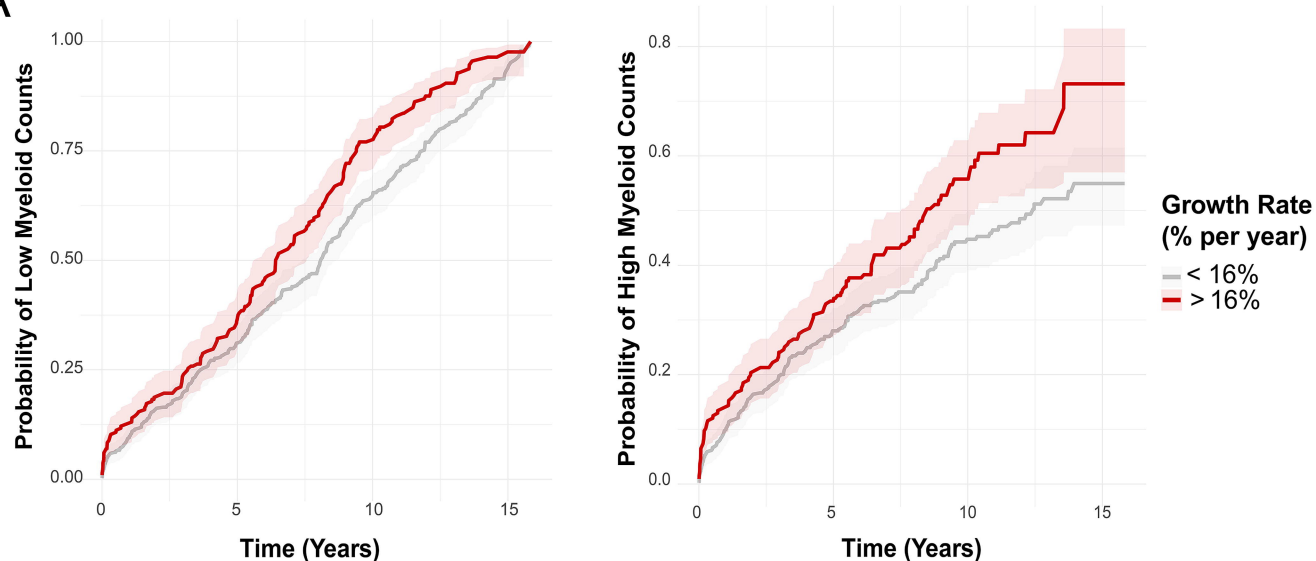
(C) Heatmap showing Clonal Hematopoiesis Risk Score (CHRS) category at the first blood draw (TP1) versus risk at second blood draw (TP2) for N=134 individuals with data available to compute a CHRS (blood counts, mean corpuscular volume, and red cell distribution width). As per Weeks et al⁴³, low risk was defined as $CHRS \leq 9.5$, intermediate risk as $10 < CHRS < 12$, and high risk as $CHRS \geq 12.5$. Darker hues represent higher numbers of individuals, and exact counts are displayed for each category.

(D) Heatmap showing the change in each of the CHRS criteria for the N=30 individuals that shifted into a different risk category between first and second blood draw. The x-axis represents each individual and the y-axis represents the CHRS components, which are faceted based on what clinical test would need to be performed to ascertain that information (i.e., none, blood panel, and sequencing). The color of the box represents the direction of the change (red is positive and blue is negative) and the darkness of the hue represents the magnitude of the change.

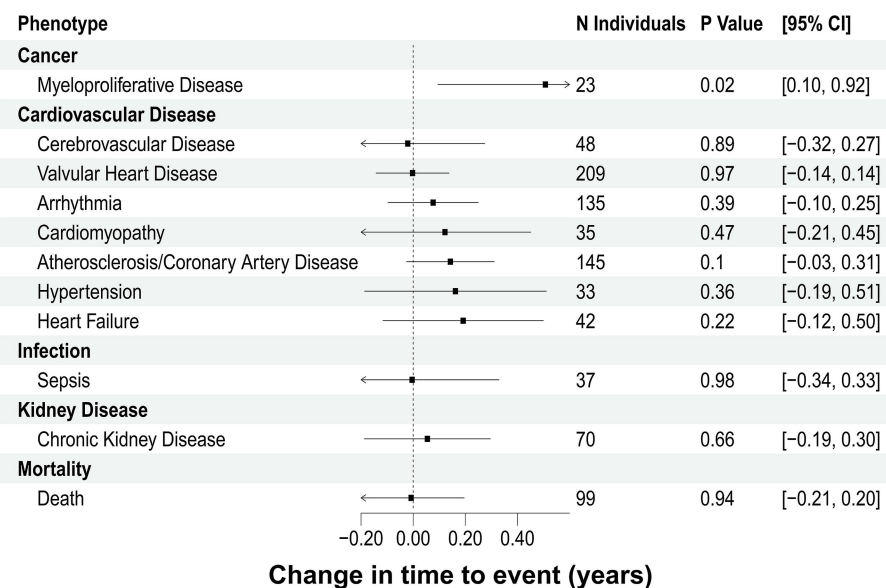


A**B****C****D****E**

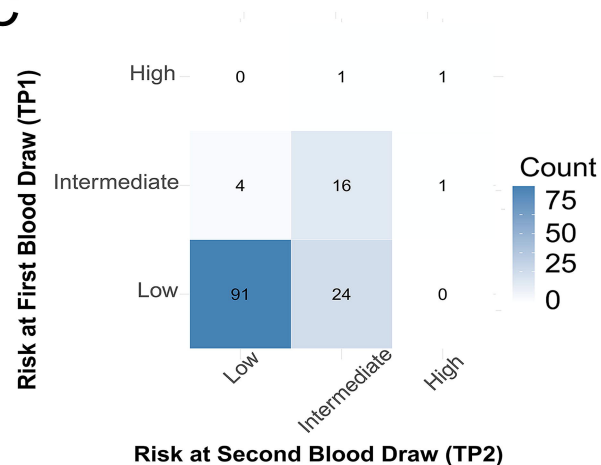
A



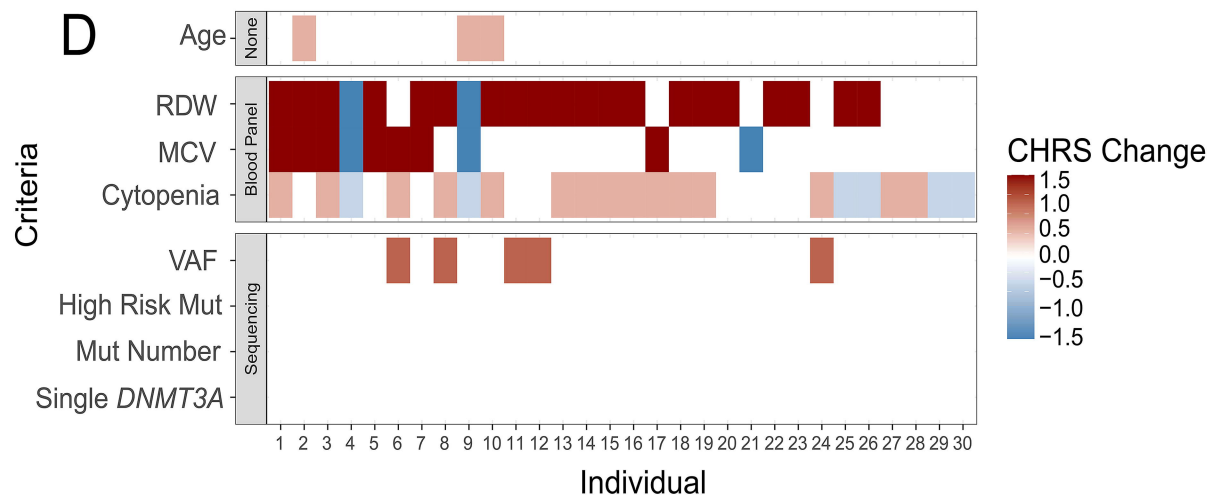
B

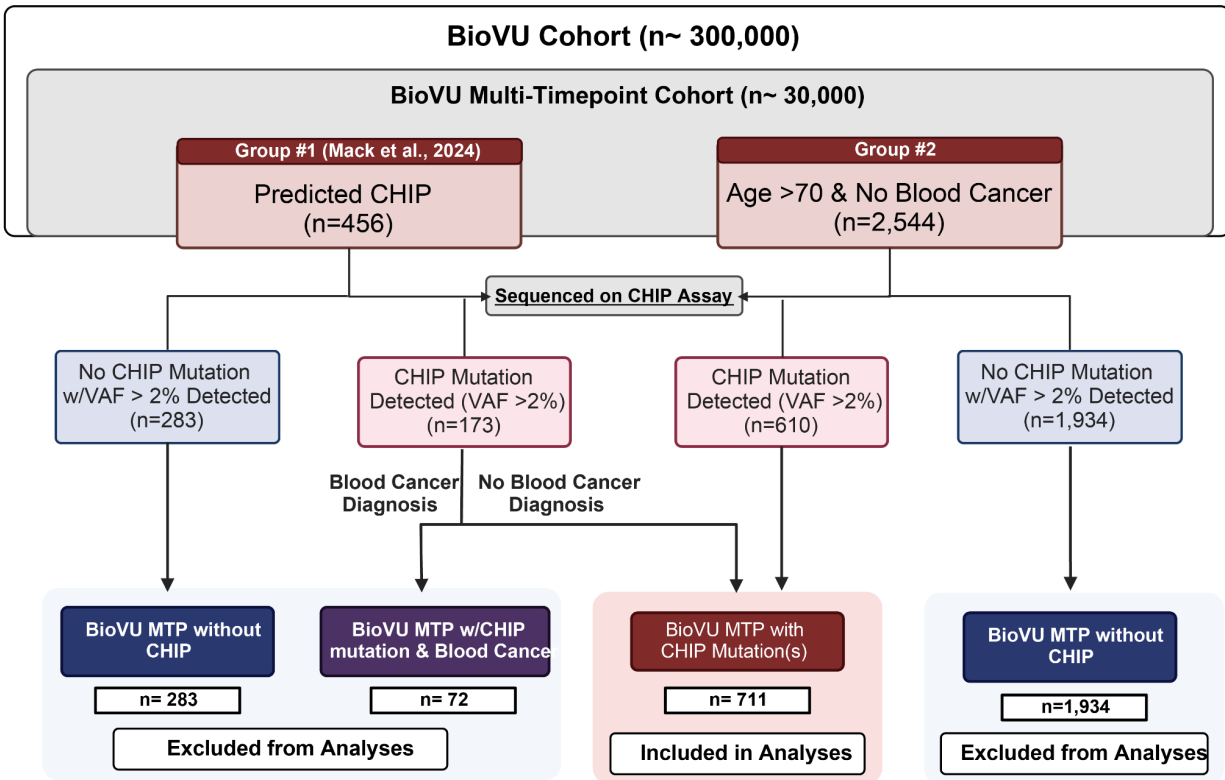


C



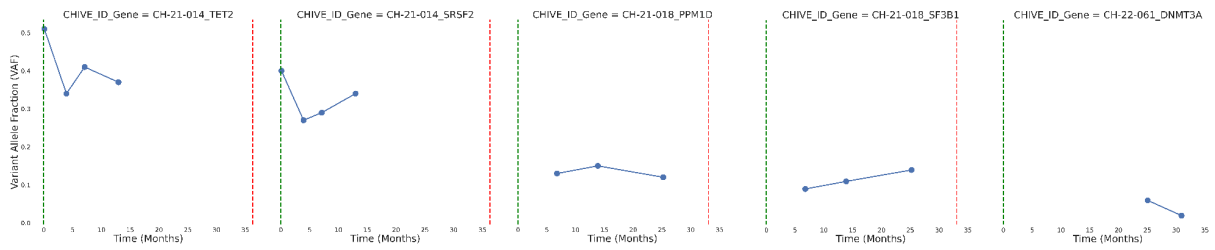
D



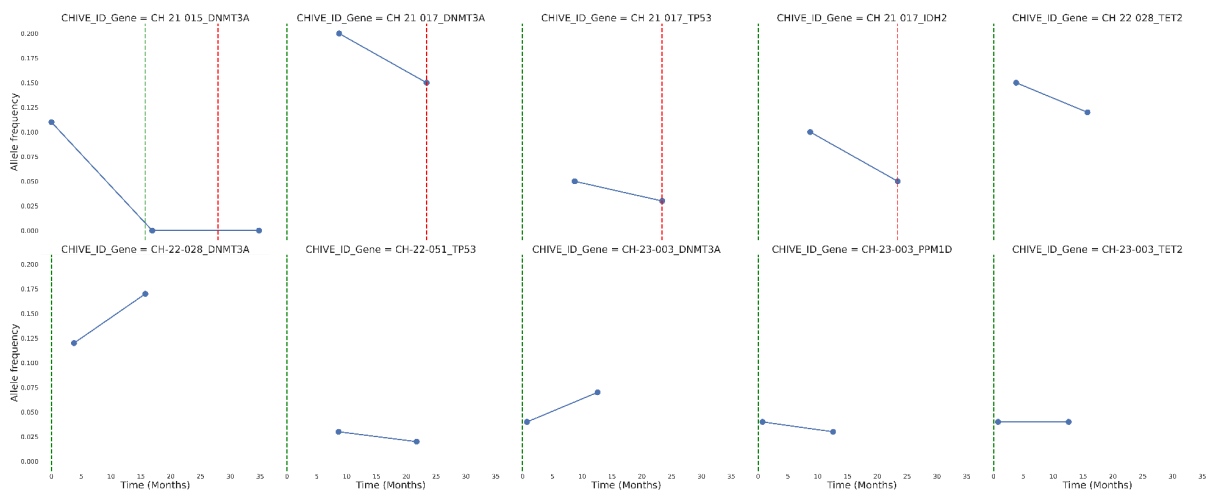


Supplementary Figure 1: Flowchart representing patient selection criteria for inclusion in the study. CHIP = Clonal hematopoiesis of indeterminate potential. MTP = multiple time point. VAF = variant allele fraction. Mack et al, 2024 is reference 6 in the manuscript.

A - Colchicine



B - Methylprednisolone



Supplementary Figure 2: (A) Clonal trajectories of 6 clones in 4 individuals with multiple sequencing blood draws while taking colchicine plotting variant allele frequency (VAF) over time in months from the Clonal Hematopoiesis and Inflammation in the Vasculature (CHIVE) cohort. Green dotted line represents the starting of colchicine. Red dotted line represents the discontinuation of colchicine. Patient ID and CHIP driver gene is shown in each subfigure title. (B) Clonal trajectories of 10 clones in 5 individuals with multiple sequencing blood draws while taking oral methylprednisolone plotting variant allele frequency (VAF) over time in months from the Clonal Hematopoiesis and Inflammation in the Vasculature (CHIVE) cohort. Green dotted line represents the starting of methylprednisolone. Red dotted line represents the discontinuation of methylprednisolone. Patient ID and CHIP driver gene is shown in each subfigure title.

Supplementary Table 1: Targeted Capture regions for identifying a CHIP mutation. Genomic coordinates are provided per the hg38 reference genome.

Chromosome	Start	Stop	Gene
chr1	1806469	1806543	<i>GNB1</i>
chr1	1815750	1815867	<i>GNB1</i>
chr1	43349257	43349363	<i>MPL</i>
chr1	114713799	114713978	<i>NRAS</i>
chr1	114716047	114716162	<i>NRAS</i>
chr2	25749689	25750420	<i>ASXL2</i>
chr2	25753532	25753640	<i>ASXL2</i>
chr2	25246614	25246781	<i>DNMT3A</i>
chr2	25313907	25313989	<i>DNMT3A</i>
chr2	25234273	25234425	<i>DNMT3A</i>
chr2	25235701	25235830	<i>DNMT3A</i>
chr2	25236930	25237010	<i>DNMT3A</i>
chr2	25239124	25239220	<i>DNMT3A</i>
chr2	25239484	25239518	<i>DNMT3A</i>
chr2	25240296	25240455	<i>DNMT3A</i>

chr2	25240634	25240735	<i>DNMT3A</i>
chr2	25241556	25241712	<i>DNMT3A</i>
chr2	25243892	25243987	<i>DNMT3A</i>
chr2	25244149	25244343	<i>DNMT3A</i>
chr2	25244534	25244657	<i>DNMT3A</i>
chr2	25245247	25245337	<i>DNMT3A</i>
chr2	25246014	25246069	<i>DNMT3A</i>
chr2	25246154	25246314	<i>DNMT3A</i>
chr2	25247045	25247163	<i>DNMT3A</i>
chr2	25247585	25247754	<i>DNMT3A</i>
chr2	25248031	25248257	<i>DNMT3A</i>
chr2	25249651	25249729	<i>DNMT3A</i>
chr2	25251906	25252099	<i>DNMT3A</i>
chr2	25252188	25252202	<i>DNMT3A</i>
chr2	25274935	25275092	<i>DNMT3A</i>
chr2	25275494	25275548	<i>DNMT3A</i>
chr2	25282382	25282716	<i>DNMT3A</i>
chr2	25300133	25300248	<i>DNMT3A</i>

chr2	208243524	208243601	<i>IDH1</i>
chr2	208248358	208248421	<i>IDH1</i>
chr2	197400709	197400941	<i>SF3B1</i>
chr2	197401979	197402135	<i>SF3B1</i>
chr2	197405269	197405477	<i>SF3B1</i>
chr2	197416735	197416916	<i>SF3B1</i>
chr2	197400049	197400171	<i>SF3B1</i>
chr2	197400246	197400439	<i>SF3B1</i>
chr2	197401394	197401530	<i>SF3B1</i>
chr2	197401736	197401893	<i>SF3B1</i>
chr2	197402550	197402831	<i>SF3B1</i>
chr2	197402943	197403040	<i>SF3B1</i>
chr2	197403579	197403769	<i>SF3B1</i>
chr2	197405070	197405182	<i>SF3B1</i>
chr2	197407992	197408124	<i>SF3B1</i>
chr2	197408363	197408586	<i>SF3B1</i>
chr2	197409764	197410012	<i>SF3B1</i>
chr4	54727217	54727324	<i>KIT</i>

chr4	54733069	54733192	<i>KIT</i>
chr4	54727415	54727542	<i>KIT</i>
chr4	54727822	54727927	<i>KIT</i>
chr4	54728010	54728121	<i>KIT</i>
chr4	54729334	54729485	<i>KIT</i>
chr4	54731327	54731419	<i>KIT</i>
chr4	54731870	54731998	<i>KIT</i>
chr4	54736497	54736609	<i>KIT</i>
chr4	105233891	105237445	<i>TET2</i>
chr4	105243564	105243783	<i>TET2</i>
chr4	105269604	105269752	<i>TET2</i>
chr4	105275042	105276524	<i>TET2</i>
chr4	105241333	105241438	<i>TET2</i>
chr4	105242828	105242932	<i>TET2</i>
chr4	105259613	105259774	<i>TET2</i>
chr4	105261753	105261853	<i>TET2</i>
chr4	105272558	105272923	<i>TET2</i>
chr9	5076681	5076701	<i>JAK2</i>

chr9	5073683	5073800	<i>JAK2</i>
chr11	119278160	119278302	<i>CBL</i>
chr11	119278504	119278718	<i>CBL</i>
chr12	22671265	22671359	<i>ETNK1</i>
chr12	25225612	25225772	<i>KRAS</i>
chr12	25227220	25227424	<i>KRAS</i>
chr12	25245270	25245384	<i>KRAS</i>
chr15	90088655	90088758	<i>IDH2</i>
chr17	60656593	60656846	<i>PPM1D</i>
chr17	60662989	60663557	<i>PPM1D</i>
chr17	7669603	7669695	<i>TP53</i>
chr17	7670603	7670720	<i>TP53</i>
chr17	7673213	7673271	<i>TP53</i>
chr17	7673301	7673344	<i>TP53</i>
chr17	7673529	7673613	<i>TP53</i>
chr17	7673695	7673842	<i>TP53</i>
chr17	7674175	7674295	<i>TP53</i>
chr17	7674814	7674976	<i>TP53</i>

chr17	7675047	7675243	<i>TP53</i>
chr17	7675988	7676277	<i>TP53</i>
chr17	7676376	7676408	<i>TP53</i>
chr17	7676515	7676627	<i>TP53</i>
chr18	44951903	44952002	<i>SETBP1</i>
chr20	32358770	32358837	<i>ASXL1</i>
chr20	32359741	32359796	<i>ASXL1</i>
chr20	32366378	32366472	<i>ASXL1</i>
chr20	32369006	32369128	<i>ASXL1</i>
chr20	32428122	32428253	<i>ASXL1</i>
chr20	32428319	32428427	<i>ASXL1</i>
chr20	32429332	32429436	<i>ASXL1</i>
chr20	32429895	32430058	<i>ASXL1</i>
chr20	32431315	32431489	<i>ASXL1</i>
chr20	32431577	32431684	<i>ASXL1</i>
chr20	32432874	32432990	<i>ASXL1</i>
chr20	32433278	32433922	<i>ASXL1</i>
chr20	32434426	32437343	<i>ASXL1</i>

chr20	58910677	58910834	<i>GNAS</i>
chr20	58909344	58909428	<i>GNAS</i>
chr20	58909515	58909584	<i>GNAS</i>
chr20	58909678	58909809	<i>GNAS</i>
chr20	58909945	58910086	<i>GNAS</i>
chr20	58910328	58910406	<i>GNAS</i>
chr21	43094649	43094793	<i>U2AF1</i>
chr21	43093096	43093254	<i>U2AF1</i>
chr21	43094461	43094568	<i>U2AF1</i>
chr21	43095432	43095541	<i>U2AF1</i>
chr21	43095688	43095748	<i>U2AF1</i>
chr21	43100447	43100524	<i>U2AF1</i>
chr21	43101274	43101437	<i>U2AF1</i>
chr21	43104309	43104407	<i>U2AF1</i>
chr21	43107445	43107499	<i>U2AF1</i>
chrX	155071527	155071650	<i>BRCC3</i>
chrX	155072326	155072343	<i>BRCC3</i>